DELPHI Collaboration

DELPHI-2001-096 CONF 524
June 25, 2001

Measurement of the production of the four-fermion final states mediated by neutral current processes

Preliminary

A. Lipniacka
Fysikum, University of Stockholm
K. Cieslik, H. Palka, M. Witek
Institute of Nuclear Physics, Krakow (supported in part by KBN Grant 2 P03B 111 16)
P. Bambade, G. Borisov
LAL, Orsay
M. Boonekamp
CEA, Saclay
M. E. Pol
CBPF, Rio De Janeiro
M. Begalli, L.M. Mundim
UERJ, Rio De Janeiro
A. Baroncelli, A. Di Simone, E. Graziani, A. Passeri, L.Pieri
Universitá di Roma TRE and INFN sez. Roma 3, Rome, Italy

Abstract

We report on measurements of the four-fermion final states originating from neutral current processes in the data sample collected by the DELPHI detector at centre-of-mass energies ranging from 183 to 208 GeV. The measurements cover a wide range of the possible final four-fermion configurations: purely leptonic ($l^+l^-l^+l^-$), hadronic and leptonic ($e^+e^-q\bar{q}$, $\mu^+\mu^-q\bar{q}$), monojet ($\nu\bar{\nu}q\bar{q}$) and hadronic final states ($q\bar{q}q\bar{q}$ with low mass $q\bar{q}$ pair).

The preliminary measurements of the cross-sections for the production of the various final states have been compared with the Standard Model expectations. The $Z\gamma^*$ contribution to all these channels was estimated.

Contributed Paper for EPS HEP 2001 (Budapest) and LP01 (Rome)

1 Introduction

Four-fermion processes become increasingly important in e^+e^- interactions as the centre-of-mass energy increases. LEP has provided a unique opportunity to verify Standard Model predictions for four-fermion interactions in several energy domains. Moreover, such processes form an irreducible background to new particle searches at LEP2 and a deviation from the Standard Model expectation would be a signal of new physics.

In this paper we report on the observation of four-fermion final states originating from neutral current processes in the data sample collected at centre-of-mass energies from 183 GeV to 208 GeV and compare our observations with the Standard Model expectations. This paper contains an update of the results presented in [1], [2], [3] and [4]. ZZ production cross-section measurements have been reported elsewhere [5]. The final states considered in the paper are $l^+l^-q\bar{q}$ ($l \equiv e^{\pm}, \mu^{\pm}$), $l^+l^-l^+l^-$, $\nu\bar{\nu}q\bar{q}$ and $q\bar{q}q\bar{q}$; data are compared with the expectations of the Standard Model in the region of 4-fermion phase space defined in table 1. [1] For all these channels, a preliminary determination of the cross-section for the $Z\gamma^*$ process has been carried out; the definition of the $Z\gamma^*$ samples is given in the relevant sections (4, 5, 6, 7).

In all the analyses presented the background from neutral current four-fermion processes outside the selections presented in table 1 was verified to be negligible.

Whenever there are no electrons in the final state the neutral-current four-fermion processes are dominated by the NC08 set of diagrams corresponding to ZZ (NC02), $Z\gamma*$ and $\gamma^*\gamma^*$ (NC06) processes. Outside the on-shell ZZ region, neutral-current four-fermion processes can be shown to be dominated by $Z\gamma^*$ production; interference effects are small in this case. The cross-section for $Z\gamma^*$ production depends strongly on the mass of the γ^*, reaching close to 120 pb for the real γ (at $\sqrt{s}$=200 GeV, integrated over all possible γ momenta). Thus a measurement of this cross-section has to be performed for a specific selection on the γ^* mass. However, the $Z\gamma^*$ cross-section depends only weakly on the centre-of-mass energy. For the $\mu^+\mu^-q\bar{q}$ final state, for example, it varies from 0.118 pb at $\sqrt{s}$=183 GeV to 0.091 pb at $\sqrt{s}$=206 GeV for the mass selections in the table 1, with an average value of 0.098 pb. For final states with electrons, other processes such as t-channel γ exchange accompanied by Z^*/γ^*-strahlung contribute significantly.

So far, there is no dedicated estimation of the theoretical uncertainties of the Standard Model cross-sections for the production of neutral-current mediated four-fermion final states outside the on-shell ZZ region. However, for most of processes discussed in this paper these uncertainties are expected to be much smaller than the statistical errors of the measurements.

2 Detector description

A summary of the properties of the DELPHI detector relevant to this analysis is presented below. A more detailed description can be found in [6].

Charged particle tracks were measured in a system of cylindrical tracking chambers

[1] The definitions in table 1 differ from those in references [2, 3, 4] in particular by the cut on $|\cos\theta_{f^{\pm}}|$ imposed on all final state charged fermions.

immersed in a 1.2 T solenoidal magnetic field. These were the Microvertex Detector (VD), the Inner Detector (ID), the Time Projection Chamber (TPC), and the Outer Detector (OD). In addition, two planes of drift chambers aligned perpendicular to the beam axis (Forward Chambers A and B) tracked particles in the forward and backward directions, covering polar angles $11^\circ < \theta < 33^\circ$ and $147^\circ < \theta < 169^\circ$.

The electromagnetic calorimetry consisted of the High density Projection Chamber (HPC) covering the barrel region of $40^\circ < \theta < 140^\circ$, the Forward ElectroMagnetic Calorimeter (FEMC) covering $11^\circ < \theta < 36^\circ$ and $144^\circ < \theta < 169^\circ$ and the STIC, a Scintillator TIle Calorimeter which extends the coverage down to 1.66° in the forward and backward regions. The 40° taggers were a series of single-layer lead-scintillator counters used to veto electromagnetic particles otherwise missed in a region between HPC and FEMC. The hadron calorimeter (HCAL) covered 98% of the solid angle. Muons with momenta above 2 GeV pass through the HCAL and were recorded in a set of Muon Drift Chambers.

3 Data samples

In this paper the integrated luminosity of 659 pb^{-1} collected by the DELPHI detector at centre-of-mass energy from 182.7 to 208 GeV was used. The luminosities collected at various centre-of-mass energies were : 55 pb^{-1} at 182.7 GeV, 158 pb^{-1} at 188.6 GeV, 25 pb^{-1} at 191.6 GeV, 77 pb^{-1} at 195.5 GeV, 82 pb^{-1} at 199.5 GeV, 41 pb^{-1} at 201.6 GeV and 221 pb^{-1} at 204-208 GeV . The data collected at 182.7 GeV were not used in the $\nu\bar{\nu}q\bar{q}$ analysis.

Simulated events were produced with the DELPHI simulation program `DELSIM`[7] and were then passed through the same reconstruction chain as the data. Processes leading to four-fermion final states were generated with `EXCALIBUR`[8], relying on `JETSET` 7.4 [9] for quark hadronisation. `EXCALIBUR` includes all tree-level diagrams in a consistent fashion. Initial state radiation was treated using the QEDPS program[10] for those final states which did not include e^+e^- pairs; for final states including e^+e^- the default `EXCALIBUR` collinear treatment was used.

Cuts were imposed at generator level on the polar angle of final state charged fermions (to make them visible inside the detector), on the invariant mass of fermion-antifermion pairs, and on $\cos\theta_e$, the cosine of the angle of electrons relative to the electron beam and positrons relative to the positron beam. This was necessary because `EXCALIBUR` treats all fermions as having zero mass and hence the cross-sections diverge unless suitable cuts are applied. The requirements used here are shown in table 1.

`GRC4F` was used to generate four-fermion final states possible in the processes of $We\nu_e$ production with $\cos\theta_e > 0.9999$, and Zee production with $\cos\theta_e > 0.98$ of one of the electrons. The background from Zee production with $\cos\theta_e > 0.98$ of both electrons was estimated with `PYTHIA` [9].

The background processes $\mathrm{e^+e^-} \to \mathrm{f\bar{f}}(n\gamma)$ were generated using `PYTHIA` [9]. Two-photon interactions were generated using `TWOGAM` [11] and `BDK` [12].

Quantity	Requirement
$\cos\theta_e$	< 0.98 in $e^+e^-f^+f^-$
$\cos\theta_e$	< 0.9999 otherwise
$\lvert\cos\theta_{f^\pm}\rvert$	< 0.98
$E(e)$	> 1.0 GeV in $e^+e^-f^+f^-$ only
$M(e^+e^-)$	> 0.05 GeV/c^2
$M(\mu^+\mu^-)$	> 0.21 GeV/c^2
$M(\tau^+\tau^-)$	> 3.6 GeV/c^2
$M(d\bar{d})$	> 2 GeV/c^2
$M(u\bar{u})$	> 2 GeV/c^2
$M(s\bar{s})$	> 2 GeV/c^2
$M(c\bar{c})$	> 5 GeV/c^2
$M(b\bar{b})$	> 15 GeV/c^2

Table 1: Requirements imposed at generator level on electron/positron angles, charged fermion angles and masses of fermion-antifermion pairs for the EXCALIBUR samples used in the analysis at centre-of-mass energies from 182.7 to 208 GeV.

4 Jets and a pair of isolated leptons

In this section the signal is defined as all $l^+l^-q\bar{q}$ events fulfilling the requirements described in section 3, table 1. The two final state leptons in the process $e^+e^- \to l^+l^-q\bar{q}$ are typically well isolated from all other particles. This property can be used to select such events with high efficiency in both muon and electron channels[2]. Events were selected initially without explicit cuts on the masses of the final state fermion pairs in order to select ZZ, $Z\gamma^*$ events and other possible diagrams contributing like Ze^+e^- or t-channel γ exchange with Z^*/γ^*-strahlung. Mass cuts were then applied to isolate the $Z\gamma*$ component.

The selection procedure for the $\mu^+\mu^-q\bar{q}$ and $e^+e^-q\bar{q}$ channels is almost the same and differs mainly in the numerical values of applied cuts. The selection procedure used for the data collected at 188.6 GeV was applied without major changes; its detailed description can be found in [3].

4.1 Results for the $l^+l^-q\bar{q}$ final state

The numbers of events observed before and after the mass selection are shown in table 2.

The observed distributions of the masses of the lepton and jet pairs for the $\mu^+\mu^-q\bar{q}$ and $e^+e^-q\bar{q}$ channels are shown in figure 1. The presence of the $Z\gamma^*$ contribution can be enhanced by requiring that one of the masses is close to M_Z [3]. If the mass of the hadronic system is required to be close to M_Z the mass distribution of the $\mu\mu$ pair has two distinct

[2]Events with $\tau^+\tau^-$ pairs are not considered here.

[3]For events with muons M_{qq} was to be in the range $M_Z - 14\ GeV/c^2 < M_{qq} < M_Z + 18\ GeV/c^2$. $M_{\mu\mu}$ was to be in the range: $M_Z - 16\ GeV/c^2 < M_{\mu\mu} < M_Z + 12\ GeV/c^2$. For events with electrons M_{qq} had to be in the range $M_Z - 12\ GeV/c^2 < M_{qq} < M_Z + 20\ GeV/c^2$ and M_{ee} was to be in the range $M_Z - 22\ GeV/c^2 < M_{ee} < M_Z + 10\ GeV/c^2$.

peaks, one close to zero and one close to M_Z, as shown in the upper left-hand picture in figure 1. For the $e^+e^-q\bar{q}$ final states, there are less events predicted with M_{ee} close to zero, and the mass distribution is flatter (lower left-hand picture in figure 1) indicating the presence of non-resonant diagrams. The predicted and observed mass distributions for the quark pair when the mass of the lepton pair is close to M_Z are shown in the right-hand side of figure 1. As expected, there are very few events with $M_{qq} < 30$ GeV/c^2 and M_{ll} close to M_Z, demonstrating the dominance of the ZZ contribution over $Z\gamma^*$ for $Z \to l^+l^-$.

Energy(GeV)	$\mu^+\mu^-q\bar{q}$			$e^+e^-q\bar{q}$		
	Data	Signal	Background	Data	Signal	Background
182.7	10	3.9 ± 0.1	0.21 ± 0.04	6	3.9 ± 0.2	0.5 ± 0.1
188.6	14	13.3 ± 0.2	0.9 ± 0.1	16	13.1 ± 0.3	1.7 ± 0.2
191.6-201.6	16	21.1 ± 0.2	1.1 ± 0.1	37	21.6 ± 0.2	2.3 ± 0.2
204-208	24	21.3 ± 0.2	1.2 ± 0.1	28	23.1 ± 0.2	3.6 ± 0.2

Table 2: The predicted numbers of signal and background events and the observed numbers of events in the $\mu^+\mu^-q\bar{q}$ and $e^+e^-q\bar{q}$ channel at centre-of-mass energies from 182.7-208 GeV. The errors quoted are from simulation statistics.

The $\mu^+\mu^-q\bar{q}$ final states with a low mass $\mu^+\mu^-$ pair are dominated by the $Z\gamma^*$ process. Also, the $\mu^+\mu^-q\bar{q}$ final states lend themselves well to a decomposition in terms of Abelian conversion diagrams $Z\gamma^*$, ZZ and $\gamma^*\gamma^*$ because of the negligible interference contribution and the negligible contribution from other processes. In the case of $e^+e^-q\bar{q}$, the contribution of the Ze^+e^- and other t-channel diagrams must be taken into account: they will be referred to as *other* $t-$*channel* components in the following.

To separate ZZ , $Z\gamma^*$, $\gamma^*\gamma^*$ and *other* $t-$*channel* contributions, a binned likelihood fit was performed to the observed distributions of the events in the ($M_{\mu^+\mu^-}$, M_{qq}) and ($M_{e^+e^-}$, M_{qq}) plane.

The `EXCALIBUR` Monte Carlo generator was used to compute expected two-dimensional distributions of events which passed the selection procedure described in section 4 and which originated from ZZ , $Z\gamma^*$ and $\gamma^*\gamma^*$ processes: $ZZ(M_{l^+l^-}, M_{qq})$, $Z\gamma^*(M_{l^+l^-}, M_{qq})$ and $\gamma^*\gamma^*(M_{l^+l^-}, M_{qq})$. The contribution originating from *other* $t-$*channel* components was used in the case of $e^+e^-q\bar{q}$ events. The small interference terms were neglected. The expected distribution of background events was also computed as $BG(M_{l^+l^-}, M_{qq})$.

The average efficiencies for the different components and for the $\mu^+\mu^-q\bar{q}$ and $e^+e^-q\bar{q}$ selections are shown in table 3.

selection	Zγ^*	$\gamma^*\gamma^*$	ZZ	t-channel
$\mu^+\mu^-q\bar{q}$	.413	.527	.964	
$e^+e^-q\bar{q}$	.256	.157	.853	.277

Table 3: Average efficiencies for the different components and for the $\mu^+\mu^-q\bar{q}$ and $e^+e^-q\bar{q}$ selections.

The five distributions were then used as an input to perform a simultaneous likelihood fit to the distributions of the data events D in the ($M_{\mu^+\mu^-}$, M_{qq}) and ($M_{e^+e^-}$, M_{qq}) planes where the free parameters were the cross-sections of the ZZ , $Z\gamma^*$, $\gamma^*\gamma^*$ contributions and *other* $t-channel$ processes giving the corresponding final state and lepton universality was assumed. The numbers of events arising from the background contribution, N_{BG}, were fixed to those predicted by the simulation, 2.0 and 8.3 events in the $\mu^+\mu^- q\bar{q}$ and $e^+e^- q\bar{q}$ samples respectively.

$D(M_{\mu^+\mu^-}, M_{qq})_{data} =$
$\sigma_{ZZ} * \epsilon_{ZZ} * ZZ(M_{\mu^+\mu^-}, M_{qq})+$
$\sigma_{Z\gamma^*} * \epsilon_{Z\gamma^*} * Z\gamma^*(M_{\mu^+\mu^-}, M_{qq})+$
$\sigma_{\gamma^*\gamma^*} * \epsilon_{\gamma^*\gamma^*} * \gamma^*\gamma^*(M_{\mu^+\mu^-}, M_{qq})+$
$\mathrm{N}_{BG} * BG(M_{\mu^+\mu^-}, M_{qq})$,

$D(M_{e^+e^-}, M_{qq})_{data} =$
$\sigma_{ZZ} * \epsilon_{ZZ} * ZZ(M_{e^+e^-}, M_{qq})+$
$\sigma_{Z\gamma^*} * \epsilon_{Z\gamma^*} * Z\gamma^*(M_{e^+e^-}, M_{qq})+$
$\sigma_{other\ t-channel} * \epsilon_{other\ t-channel} * other\ t-channel(M_{e^+e^-}, M_{qq})+$
$\sigma_{\gamma^*\gamma^*} * \epsilon_{\gamma^*\gamma^*} * \gamma^*\gamma^*(M_{e^+e^-}, M_{qq})+$
$\mathrm{N}_{BG} * BG(M_{e^+e^-}, M_{qq})$.

The following average luminosity-weighted preliminary cross-sections for $\mu^+\mu^- q\bar{q}$ and $e^+e^- q\bar{q}$ production (assuming lepton universality) were obtained:

$\sigma_{Z\gamma^*} = 0.129 \pm 0.020(\mathrm{stat})$ pb

$\sigma_{ZZ} = 0.029 \pm 0.006(\mathrm{stat})$ pb

$\sigma_{\gamma^*\gamma^*} = 0.017 \pm 0.008(\mathrm{stat})$ pb and

$\sigma_{t-channel} = 0.245 \pm 0.045(\mathrm{stat})$ pb

The systematic errors on the $Z\gamma^*$ cross-section measurement are briefly discussed below. The limited Monte Carlo statistics of the generated signal and background samples accounted for ± 0.005 pb. The effect of varying the selection cuts used in the analysis was evaluated by choosing an alternative selection giving the same statistical error. The corresponding variation of the measured cross-section was found to be ± 0.0005 pb. The systematic uncertainty due to the knowledge of the background was evaluated by comparing Monte Carlo events and data in which selected muons were required not to be isolated. The simulated sample thus selected contained only 3% of signal events. The observed data - Monte Carlo difference induced a variation in the cross-section measurement which amounts to ± 0.006 pb. The total estimated systematic error was thus ± 0.008 pb. This gave

$\sigma_{Z\gamma^*} = 0.129 \pm 0.020(\text{stat}) \pm 0.008(\text{syst})$ pb and

$\sigma_{ZZ} = 0.029 \pm 0.006(\text{stat})$ pb.

These results are luminosity weighted average cross-sections and are in agreement with the corresponding EXCALIBUR prediction (luminosity weighted average cross-sections as well) of: $\sigma_{Z\gamma^*} = 0.098$ pb and $\sigma_{ZZ} = 0.035$ pb.

The two projections of the fitted mass distribution along M_{qq} and $M_{\mu^+\mu^-}$ are shown in figure 1.

5 Four leptons

There are six possible four-lepton final states: $e^+e^-e^+e^-$, $e^+e^-\mu^+\mu^-$, $e^+e^-\tau^+\tau^-$, $\mu^+\mu^-\mu^+\mu^-$, $\mu^+\mu^-\tau^+\tau^-$ and $\tau^+\tau^-\tau^+\tau^-$. Two types of analyses are reported here. In the first analysis no attempt has been made to identify lepton flavour in the final state ("flavour blind analysis"). The second analysis was directed to identify specifically $e^+e^-\mu^+\mu^-$ final states. In both analyses the signal is defined as all four-fermion processes giving corresponding final states within the selections listed in table 1, i.e. all four charged lepton final states for the flavour blind analysis and the $e^+e^-\mu^+\mu^-$ final state for the second analysis. The total cross-sections were obtained for both selections. For the flavour-blind analysis the measurement of the ZZ and $Z\gamma^*$ contributions was attempted.

The $l^+l^-l^+l^-$ final states were reported in the earlier note [3] and the analyses presented there were used without major modifications in the present paper, except that the analysis was narrowed to the phase-space region where all the leptons can be registered in the detector, by requiring that for each lepton the cosine of the polar angle fulfils the condition $|\cos(\theta)| \leq 0.98$.

The event selection for both analyses has been restricted to topologies with four well reconstructed charged particles with momenta greater than 2 GeV/c (called henceforth lepton candidates). Only one additional well measured charged particle was allowed, provided that its momentum was less than 2 GeV/c , and another five charged particles were permitted if the tracks did not point to the vertex, implying that in the $e^+e^-\tau^+\tau^-$, $\mu^+\mu^-\tau^+\tau^-$ and $\tau^+\tau^-\tau^+\tau^-$ cases only one-prong decays of the τ were considered. The sum of charges of the lepton candidates had to be equal to zero and the angle between momentum directions of any two of them had to be larger than 5°. A search for two nearby tracks with opposite charge was performed in order to eliminate γ conversions.

5.1 Flavour blind analysis

The four-lepton candidates had to fulfil the following additional selection criteria, namely: the total energy carried by them had to be greater than 50 GeV to reject background from two-photon interactions; the track length of at least two lepton candidates had to be greater than 50 cm to eliminate events reconstructed only with VD-ID tracks; and it was required that the four charged particles were not collinear in θ in order to minimize the background from $\tau^+\tau^-(\gamma)$ final states. To further eliminate gamma conversions,

the invariant mass of the pair of oppositely charged lepton candidates with the smallest opening angle was required to be greater than 1.2 GeV/c^2.

The efficiency for this selection and the expected signal were extracted from EXCALIBUR Monte Carlo for the six processes under study, where a cut $|\cos(\theta)| \leq 0.98$ was imposed on the polar angle of every lepton. The background from outside this polar region was negligible.

The Monte Carlo simulations used to estimate the background included two-fermion final states, two-photon interactions and all other four-fermion processes, simulated as described in the section 3.

The expected numbers of events for signal and background for the "flavour blind" four lepton analysis, together with the numbers of events found in the data are shown in table 4. The efficiencies for the $\ell^+\ell^-\ell^+\ell^-$ selection are 8.5±0.6 %, 9.7±0.6 %, 12.0±0.3 % and 11.8±0.2 % for the centre-of-mass energies of 182.7 GeV, 188.6 GeV, 192-202 GeV and 204-209 GeV, respectively.

The most important contribution to the background was found to be the one coming from $e^+e^- \to e^+e^-q\bar{q}$, with low mass for the $q\bar{q}$ pair. The second most important contribution is due to $e^+e^- \to \tau^+\tau^-(\gamma)$ processes.

Channel	182.7 GeV	188.6 GeV	192-202 GeV	204-209 GeV
$\mu^+\mu^-\mu^+\mu^-$	0.23±0.04	0.87±0.13	0.99±0.05	0.92±0.04
$e^+e^-e^+e^-$	0.86±0.11	2.57±0.30	3.38±0.16	2.85±0.10
$\tau^+\tau^-\tau^+\tau^-$	0.02±0.01	0.11±0.04	0.10±0.01	0.10±0.01
$e^+e^-\mu^+\mu^-$	1.76±0.22	5.04±0.55	7.35±0.30	6.77±0.21
$e^+e^-\tau^+\tau^-$	0.47±0.04	1.35±0.13	1.58±0.07	1.58±0.06
$\mu^+\mu^-\tau^+\tau^-$	0.18±0.04	0.38±0.07	0.78±0.04	0.78±0.03
Signal	3.52±0.26	10.32±0.65	14.18±0.35	13.00±0.25
Backgr.	1.13±0.10	1.25±0.11	2.49±0.14	1.60±0.09
TOTAL	4.65±0.28	11.57±0.66	16.67±0.38	14.60±0.27
DATA	4	14	18	16

Table 4: Expected number of events for signal and background for the "flavour blind" four lepton analysis

A constrained fit was performed on the data and Monte Carlo selected events, taking into account particle identification, to calculate the masses of each pair. In figure 2 the masses of the pairs with biggest and smallest masses are shown, for all energies together.

5.2 Search for $e^+e^-\mu^+\mu^-$ final states

In the dedicated search for $e^+e^-\mu^+\mu^-$ final states, two lepton candidates of opposite charge were required to be identified as $\mu^+\mu^-$ and the other two as e^+e^-.

Muon identification was performed combining the standard DELPHI identification package in the Muon Chambers with the shower profile in the Hadron Calorimeter and the energy deposited in the Electromagnetic Calorimeter. For the Hadron Calorimeter, a

variable MUHA was defined as the sum of the energy deposited in the third and fourth layers divided by the sum of the energy deposited in the first and second layers. A charged particle was considered a muon if it satisfied at least two of the following three conditions:

- It was identified as a muon in the Muon Chambers.
- The energy deposited in the Electromagnetic Calorimeter was less than 2 GeV.
- The variable MUHA had values between 0.5 and 2.0 or the total energy deposited in the Hadron Calorimeter was less than 10 GeV.

Electron identification required that there should not be any signal in the Muon Chambers nor any energy in the Hadron Calorimeter deposited after the first layer associated to the electron candidates. The energy in the Electromagnetic Calorimeter deposited in a 2° cone surrounding the particle had to be larger than 1 GeV. For electrons satisfying these criteria, the momenta of the charged particle was replaced by the energy deposited in the Electromagnetic Calorimeter.

The efficiency and the expected numbers of events from signal and background were determined using the same sample of simulated Monte Carlo as in the "flavour blind" analysis, with the final states $\mu^+\mu^-\mu^+\mu^-$, $e^+e^-e^+e^-$, $\tau^+\tau^-\tau^+\tau^-$, $e^+e^-\tau^+\tau^-$ and $\mu^+\mu^-\tau^+\tau^-$ now considered as background. The major contribution to the four-lepton background was due to $\tau^+\tau^-\tau^+\tau^-$, while for the non-four-lepton case it originated from the $e^+e^-q\bar{q}$ and $\mu^+\mu^-(\gamma)$ final states.

The results of the selection are shown in table 5.

Channel	$e^+e^-\mu^+\mu^-$					
Energy	ϵ (%)	N_{true}	$N_{bckg-4l}$	$N_{bckg-non-4l}$	N_{total}	DATA
182.7 GeV	8.7±1.3	1.08±0.17	0.03±0.01	0.02±0.01	1.13±0.17	2
188.6 GeV	10.3±1.3	3.39±0.44	0.08±0.01	0.06±0.03	3.53±0.44	5
192-202 GeV	11.4±0.5	4.97±0.24	0.18±0.01	0.13±0.03	5.28±0.24	7
204-208 GeV	11.6±0.4	4.64±0.17	0.17±0.01	0.07±0.01	4.88±0.17	4

Table 5: Efficiencies and identified number of events expected and found for $e^+e^-\mu^+\mu^-$ final state.

In figure 3, the fitted masses of the e^+e^- and $\mu^+\mu^-$ pairs are shown for all energies together.

5.3 Total cross-sections for the four charged lepton channel

The visible cross-sections were calculated taking into account the background and efficiency.

The main sources of the systematic error were found to be those due to the differences between data and Monte Carlo for the number of reconstructed charged tracks, charge

conservation and particle identification. The contribution coming from the determination of the luminosity was also taken into account.

The total cross-sections in the region of $|\cos(\theta)| \leq 0.98$ were found to be:
For the flavour-blind analysis:

$$\sigma_{182.7GeV} = (0.61^{+0.37}_{-0.27} \pm 0.04)pb$$
$$\sigma_{188.6GeV} = (0.83^{+0.26}_{-0.22} \pm 0.06)pb$$
$$\sigma_{192-202GeV} = (0.57^{+0.15}_{-0.13} \pm 0.04)pb$$
$$\sigma_{204-208GeV} = (0.55^{+0.15}_{-0.13} \pm 0.04)pb,$$

and for the $e^+e^-\mu^+\mu^-$ final state:

$$\sigma_{182.7GeV} = (0.41^{+0.40}_{-0.27} \pm 0.03)pb$$
$$\sigma_{188.6GeV} = (0.30^{+0.18}_{-0.14} \pm 0.02)pb$$
$$\sigma_{192-202GeV} = (0.26^{+0.12}_{-0.09} \pm 0.02)pb$$
$$\sigma_{204-208GeV} = (0.15^{+0.13}_{-0.11} \pm 0.01)pb.$$

were obtained, all in good agreement with the `EXCALIBUR` visible cross-sections predictions. The first error quoted is the statistical one, while the second is the systematic error.

5.4 The $Z\gamma^*$ and ZZ contributions

In order to extract the $Z\gamma^*$ and ZZ contributions from the sample selected with the flavour blind analysis, particle identification was used to classify the final state into one of those listed in table 4 and a constrained fit was performed to calculate the masses of the pairs of oppositely charged leptons. The events were classified as $Z\gamma^*$ (ZZ) if the mass of one pair (two pairs) lay within $\pm$ 7.5 GeV/c^2 of the Z mass.

The efficiencies of the $Z\gamma^*$ (ZZ) selections described above for all four-lepton processes with one lepton pair (both lepton pairs) generated inside the $\pm$ 7.5 GeV/c^2 window from the Z mass were obtained with the EXCALIBUR simulation and are listed in tables 6 and 7 together with the corresponding numbers of the predicted signal and background events. Events originating from the four lepton processes with the masses of the lepton pairs outside the specified window were included in the background.

In order to obtain the $Z\gamma^*$ (and ZZ) contributions, the cross-sections for the four-lepton processes with one (both) lepton pair mass inside the window were corrected with a scaling factor R which takes into account other contributing four-lepton production diagrams. The scaling factor R defined as

$$R = \frac{\sigma^{total}_{Z\gamma^* or ZZ}}{\sigma^{window}_{4l}},$$

was obtained using EXCALIBUR. For ZZ the R factor is near unity, which shows that the region inside the mass window is dominated by NC02 diagrams, while for $Z\gamma^*$ R has values around 0.5 due to important contributions from the t-channel and multiperipheral diagrams.

Energy	ϵ (%)	N_{signal}	N_{bckg}	DATA	R
182.7 GeV	14.7	0.65	0.10	0	0.49
188.6 GeV	17.4	2.17	0.20	2	0.52
192-202 GeV	15.8	2.27	0.16	4	0.50
204-208 GeV	16.9	2.18	0.11	5	0.48

Table 6: Efficiencies, number of expected events from signal and background, number of selected events in data and correction factor R for the $Z\gamma^*$ selection.

Energy	ϵ (%)	N_{signal}	N_{bckg}	DATA	R
182.7 GeV	21.7	0.03	0	0	0.95
188.6 GeV	30.4	0.17	0	0	1.10
192-202 GeV	36.4	0.59	0	1	1.18
204-208 GeV	32.1	0.60	0	1	1.08

Table 7: Efficiencies, number of expected events from signal and background, number of selected events in data and correction factor R for the ZZ selection.

We thus obtained for the $Z\gamma^*$ cross-sections in the restricted polar region $|\cos(\theta)| \leq 0.98$:

$$\sigma^{Z\gamma^*}_{188.6GeV} = (0.034^{+0.026}_{-0.013})pb$$
$$\sigma^{Z\gamma^*}_{192-202GeV} = (0.053^{+0.032}_{-0.023})pb$$
$$\sigma^{Z\gamma^*}_{204-208GeV} = (0.062^{+0.033}_{-0.025})pb,$$

and for ZZ:

$$\sigma^{ZZ}_{192-202GeV} = (0.015^{+0.023}_{-0.011})pb$$
$$\sigma^{ZZ}_{204-208GeV} = (0.015^{+0.023}_{-0.011})pb$$

where only statistical errors were considered.

6 The $q\bar{q}\nu\bar{\nu}$ channel

In the $q\bar{q}\nu\bar{\nu}$ channel the ZZ contribution dominates over the $Z\gamma^*$ one. However, for $M_{q\bar{q}} < 60$ GeV/c^2, the ZZ contribution is expected to be negligible and final states have characteristic signature of "monojets", with the low invariant mass hadronic system arising from the γ^* hadronization. In the low mass region the cross-section is thus dominated by the $Z\gamma^*$ contribution. In the region 2 GeV/$c^2 < M_{q\bar{q}} < 60$ GeV/c^2 `EXCALIBUR` predicts a cross-section of 0.060 pb at 189 GeV centre-of-mass energy and 0.056 pb at 200 GeV. When the γ^* mass is close to that of the Vector Mesons, processes like $\gamma^* \rightarrow \rho \rightarrow \pi\pi$

can occur. The total cross-section for $q\bar{q}\nu\bar{\nu}$ in the region $2M_\pi < M_{q\bar{q}} < 2$ GeV/c^2 can be obtained assuming hadron-parton duality and was estimated with KORALW [13]. To model correctly final states arising in this case, non-perturbative effects have to be included (eg. Vector Meson Dominance modelling). A simplified modelling of the γ^* fragmentation was used for this purpose. It was assumed that for $2M_\pi < M_{q\bar{q}} < 2$ GeV/c^2 only $\gamma^* \to \rho \to \pi\pi$ takes place. The pion form factor measured as $R_\pi = \sigma(e^+e^- \to \pi^+\pi^-)/(e^+e^- \to \mu^+\mu^-)$ was used to model invariant mass distribution of $\pi^+\pi^-$ pairs. The total cross-section for $2M_\pi < M_{q\bar{q}} < 2$ GeV/c^2 was thus estimated to be 0.032 pb at 189 GeV centre-of-mass energy and 0.031 pb at 200 GeV centre-of-mass energy. Our preliminary estimate is that including other resonances does not change these cross-sections by more than 20%. This was checked by using a more sophisticated treatment [14], based on KORALW as well, in which contributions from resonances other than ρ (ω, Φ) and from the continuum (by compiling exclusive e^+e^- cross-sections to 3,4,5,6 π's and kaons) are also taken into account. The total $Z\gamma^*$ cross-section in the region $2M_\pi < M_{q\bar{q}} < 60$ GeV/c^2 is thus expected to vary between 0.092 pb and 0.084 pb (EXCALIBUR+KORALW), weakly dependent on the centre-of-mass energy. In this section we considered as a signal the $Z\gamma^*$ processes with $\gamma^* \to q\bar{q}$ and $Z \to \nu\bar{\nu}$. Other processes (ZZ in particular) were considered as background. The interference between $Z\gamma^*$ process with $\gamma^* \to q\bar{q}$ and $Z \to \nu\bar{\nu}$ and other processes was estimated to be negligible and neglected.

Two analyses were performed: the first one is intended to probe the low mass region of the hadronic system, thus to be efficient for M_{γ^*} below 2 GeV/c^2, where most of the cross-section is expected. The second one is intended to have a better overall efficiency at the expense of having very small efficiency in the low M_{γ^*} region. No explicit cut on the reconstructed mass was applied in any of the two analyses. These two analyses were applied and combined as described in [2] without changes.

6.1 Results

In total 45 events in data were found, while 38.3 events were expected from Standard Model, of which 17.2 from $q\bar{q}\nu\bar{\nu}$ signal process and 21.1 from background processes, mainly from WW and single $We\nu$ contributions. Table 8 shows the predicted numbers of signal and background events and the observed numbers of events in the $\nu\bar{\nu}q\bar{q}$ channel at the various centre-of-mass energies.

Energy(GeV)	$\nu\bar{\nu}q\bar{q}$		
	Data	Signal	Background
188.6	13	4.9 ± 0.1	5.9 ± 0.70
192-202	16	6.55 ± 0.03	7.8 ± 0.5
204-208	16	5.75 ± 0.03	7.4 ± 0.5

Table 8: The predicted numbers of signal and background events and the observed numbers of events in the $\nu\bar{\nu}q\bar{q}$ channel at the various centre-of-mass energies. The errors quoted are from simulation statistics.

The average efficiency, as computed in Monte Carlo for $Z\gamma^* \to q\bar{q}\nu\bar{\nu}$ events with

$M_{\gamma^*} < 60$ GeV/c^2 is (31.0 ± 0.3) %, where the error is statistical only. The efficiency as a function of the Monte Carlo generated $q\bar{q}$ mass is shown in fig. 4 (lower plot), together with the expected $q\bar{q}$ mass distribution (upper plot). The efficiency is negligible for $q\bar{q}$ mass above 60 GeV/c^2. The distribution of the reconstructed M_{γ^*} for 45 data events is shown in fig. 5. Also shown are the corresponding distributions of simulated signal and background events.

The background, as shown in table 8, was subtracted, and the average efficiency correction for $\sigma(Z\gamma^* \to q\bar{q}\nu\bar{\nu})$ with $M_{\gamma^*} < 60$ GeV/c^2 was applied. The resulting value was corrected to take into account the part of the $Z\gamma^*$ spectrum corresponding to $M_{\gamma^*} > 60\ GeV/c^2$. The correction was estimated to be 2.2%, by fitting the generated $q\bar{q}$ mass distribution in the $Z\gamma^*$ sample and extrapolating it up to the kinematical limit. No correction was applied to account for the contribution of $ZZ \to q\bar{q}\nu\bar{\nu}$ events, because the efficiency drops to zero above 60 GeV/c^2.

The result was :

$$\sigma_{Z\gamma^* \to q\bar{q}\nu\bar{\nu}} = 0.129 \pm 0.035 \text{ (stat) pb.}$$

A very preliminary estimate of systematic errors was performed. The limited Monte Carlo statistics gave an uncertainty of ± 0.008. Uncertainties coming from background subtraction were estimated by using different hadronisation models (ARIADNE vs. JETSET), different $e^+e^- \to W^+W^-$ generators (`EXCALIBUR vs. PYTHIA`), different $e^+e^- \to \gamma\gamma$ generators (TWOGAM vs BDK). Contributions to the cross-section measurement were, respectively: ± 0.003 pb, ± 0.002 pb, ± 0.002 pb. Cuts were independently varied within reasonable intervals and the width of the corresponding cross-section distribution was assumed to represent this source of systematic error: this gave ± 0.012 pb contribution on the cross-section measurement. Detector induced effects were exploited by looking at data-simulation disagreement at a level of the analysis in which the signal is negligible with respect to the background. The difference in term of absolute number of events was assumed to represent this source of systematic uncertainty and was estimated to contribute to ± 0.001 pb to the cross-section measurement. The γ^* hadronisation model in [14] was used to estimate the systematic uncertainty in the efficiency evaluation in the low $q\bar{q}$ mass region: this gave a contribution of ± 0.001 pb on the cross-section measurement. The total estimated systematic error was ± 0.015 pb.

The average luminosity weighted cross-section was thus measured to be:

$$\sigma_{Z\gamma^* \to q\bar{q}\nu\bar{\nu}} = 0.129 \pm 0.035 \text{ (stat)} \pm 0.015 \text{ (syst) pb.}$$

The Standard Model expectation of the cross-section for this process is 0.092 pb-0.084 pb (`EXCALIBUR+KORALW`, see sec. 6) for the range of centre-of-mass energies used in the analysis. This result is thus in agreement with the Standard Model prediction.

7 The $q\bar{q}q\bar{q}$ channel

The selection of $Z\gamma^*$ in the $q\bar{q}q\bar{q}$ channel has to deal with background processes like $q\bar{q}(\gamma)$ and W^+W^- which have cross-sections larger by orders of magnitude than the signal. It

is thus impossible to extract the signal in all the possible $q\bar{q}$ mass spectrum. Therefore, to enhance the $Z\gamma^*$ contribution, only a restricted mass region was considered, with the mass of one $q\bar{q}$ pair below 2 GeV/c^2 recoiling against a $q\bar{q}$ system with mass compatible with M_Z. The expected cross-section was computed and the signal was simulated in a way similar to that in sec. 6, (by using `KORALW` [13] with non-perturbative effects introduced, and with the simplified modelling of the γ^* fragmentation, including only the dominant $\gamma^* \rightarrow \rho \rightarrow \pi\pi$ process). The same considerations as in sec.6 hold in this case. The total $Z\gamma^*$ cross-section for $q\bar{q}q\bar{q}$, with one $q\bar{q}$ pair with mass $2M_\pi < M_{q\bar{q}} < 2$ GeV/c^2 was estimated to be 0.2 pb at 200 GeV centre-of-mass energy. The signal was defined by this requirement on $M_{q\bar{q}}$, plus an additional requirement on the polar direction of each generated quark: $|cos(\theta_q)| < 0.98$. The corresponding cross-sections, at 189 and 200 GeV centre-of-mass energy, were evaluated to be 0.091 pb and 0.082 pb, respectively. The cross-section at 200 GeV is close to the expected luminosity weighted cross section and will be used for comparison.

The process which was searched for in the present analysis is thus $e^+e^- \rightarrow Z\gamma^* \rightarrow qq\rho,\ \rho \rightarrow \pi^+\pi^-$, and is characterized by two jets from the decay of the Z and one highly energetic low mass jet from the ρ decay, which is preferentially directed close to the beam.

Backgrounds from $q\bar{q}(\gamma)$, W^+W-, $q\bar{q}\mu^+\mu^-$, $q\bar{q}e^+e^-$ and $q\bar{q}\tau^+\tau^-$, which are expected to give the dominant contributions, were considered.

Two analyses were performed: the first one was based on a series of optimized sequential cuts; the second one, which made use of the part of the selection developed in the first one, allowed for the determination of the background directly from the data and was used as a cross-check.

7.1 The sequential cut analysis

Events were cluseterd according to the LUCLUS [15] algorithm with the parameter d_{join} set to 6.5 GeV/c.

A set of cuts was then applied to the data, in order to extract the signal from the background. Selections listed in the following were the result of an optimization process, briefly described hereafter. Cut #1 selects hadronic events. Cuts #2 to #10 look for pairs of tracks with the desired characteristics in the events.

1. The total event charged particle multiplicity was required to be larger than 20; the ratio $\sqrt{s}'/\sqrt{s}$ had to be greater than 80%, where $\sqrt{s}'$ is the reconstructed effective centre-of-mass energy; the number of muons in the event had to be less than 3; no tracks with electromagnetic energy greater than 50 GeV were allowed; the missing energy of the event was required be less than 82% of the total energy of the event; the number of reconstructed jets had to be greater than 2. Then, it was required that the event contained at least one charged particle with momentum above 32 GeV/c: for each such particle two pairs were built, with the charged particle closest in space, and with the next-to-closest one. These pairs were then subjected to the selections below.

2. The momentum of each charged particle in the pair was required to be $p > 0.4$ GeV/c and its impact parameter to be compatible with the primary event vertex.

3. The total energy of the pair had to be larger than 64 GeV and the jet to which the pair belonged had to have charged multiplicity less than 3.

4. The sum of the electromagnetic energies of the two particles had be less than 64% of the total energy of the pair.

5. The two particles had to be of opposite charge.

6. Neither muons nor electrons were allowed in the pair (anti-lepton cut).

7. The angle between the two particles had to be less than 0.31 rad (collimation cut).

8. The angles between each charged particle in the pair and the axe of the jets of the event (not including the jet to which the pair belonged) had to be larger than 0.39 rad (isolation cut).

9. The invariant mass of the two particles had be less than 2 GeV/c^2.

10. The mass of the system recoiling against the selected charged particle pair, reconstructed with the triangle formula, had to be between 70 GeV/c^2 and 110 GeV/c^2.

When a pair passing all the cuts was found, the event was accepted.

The cuts were optimised by scanning the full range of the relevant discriminating variables and calculating, for each set of values, the cross-section and the quantity $\epsilon * purity$. Figure 6 shows the $(\epsilon\, p)$ correlation plot for 134 sets of parameters. The set has been chosen which gave the highest value of ϵp (0.105), corresponding to $\epsilon = 17.7\%$, a purity of 59.5% and a ratio $\frac{signal}{\sqrt{background}} = 3.8$.

The distribution of the cross-section obtained for different values of the cuts, corresponding to $\epsilon p > 0.08$ and $\epsilon > 16\%$, was observed to have a Gaussian behaviour and was thus fitted: the fit gave a standard deviation of 0.005 pb. This was assumed to represent the systematic error due to the choice of a particular set of values.

Table 9 shows the number of data events that pass the various selections as a function of the sequential cut, compared with the expectations of the simulation. Table 10 shows the predicted numbers of signal and background events and the observed numbers of events in the $q\bar{q}q\bar{q}$ channel at the various centre-of-mass energies.

The following result (luminosity weighted cross-section) was obtained:

$$\sigma_{Z\gamma* \to qq\rho} = 0.071 \pm 0.042(stat) \pm 0.005(syst\ cut)\ pb.$$

where the second error represents the systematics coming from the choice of the cut values. The result is in agreement with the Standard Model expectation of 0.082 pb at a centre-of-mass energy of 200 GeV.

Cut number	Data	MC total	signal	WW	QCD	$qq\mu\mu$	$qqee$	$qq\tau\tau$
1	14426	15342.7	43.6	6802.2	8329.7	80.3	40.9	46.0
2	4396	4459.7	31.4	1947.6	2358.8	72.5	32.0	17.4
3	558	609.5	16.7	470.6	63.6	45.6	11.7	1.3
4	350	372.5	13.7	287.9	24.1	38.3	7.9	0.6
5	346	364.2	13.6	283.4	23.7	38.3	4.7	0.5
6	320	336.9	13.3	267.9	23.7	27.4	4.1	0.5
7	54	53.0	12.9	8.2	19.1	11.1	1.6	0.09
8	26	31.7	12.1	6.3	8.7	2.9	1.6	0.07
9	15	20.3	10.2	4.0	3.3	1.6	1.3	0.05
10	15	16.8	10.0	2.3	2.7	0.9	0.9	0.01

Table 9: Data - Monte Carlo comparison of number of events as a function of the sequential cut in $q\bar{q}q\bar{q}$ analysis

Energy(GeV)	$q\bar{q}q\bar{q}$		
	Data	Signal	Background
182.7	3	0.8 ± 0.2	0.46 ± 0.02
188.6	5	2.4 ± 0.2	1.34 ± 0.02
192-202	3	3.3 ± 0.2	1.79 ± 0.01
204-208	3	2.9 ± 0.2	1.61 ± 0.02

Table 10: The predicted numbers of signal and background events and the observed numbers of events in the $q\bar{q}q\bar{q}$ channel at the various centre-of-mass energies. The errors quoted are from simulation statistics.

7.2 Different background evaluation

A second analysis was performed in order to check the measurement of the cross-section. The cuts on invariant mass, recoil mass, isolation and collimation were completely released (cuts #7,#8,#9, #10), and the invariant mass of the pairs of charged particles that passed the remaining cuts was calculated. In the data, 22 events were found with an invariant mass of the selected charged particle pair below 2 GeV/c^2. Figure 7 shows the simulated distribution of invariant mass for $\pi^+\pi^-$ candidate pairs for the background component only. A small peak can be seen below 2 GeV/c^2 in the mass distribution of the background: this peak comes mainly from the $q\bar{q}\gamma$ component and is probably due to the presence of real ρ and low mass virtual gluons. The distribution was fitted in the region between 0 and 10 GeV/c^2 with a simple analytic function whose form is depicted on figure 7 (χ^2/DOF=1.64). Then the corresponding data distribution was fitted with the same function between 4 and 10 GeV/c^2 (where no signal is expected), fixing all the shape parameters but a normalization factor. The integral content below 2 GeV/c^2 (where signal is expected) of the resulting function was assumed to represent an estimate of the number of background events and used to compute the cross-section. With a Monte Carlo estimated efficiency of 21.8%, the result was

$$\sigma_{Z\gamma^* \to qq\rho} = 0.090 \pm 0.033(stat)\, pb.$$

The reliability of the simulation in estimating the background was evaluated by looking at selected pairs with tracks of the same charge, thus working in an almost signal-free situation. In the data, 3 events were found with mass of the candidate $\pi^+\pi^+$and $\pi^-\pi^-$ pairs below 2 GeV/c^2, while the simulation predicted 3.75±0.5. As these numbers are compatible, the statistical error of the difference was assumed as a systematic uncertainty due to the background evaluation in the ρ region. This gave a contribution of ±0.014 pb on the cross-section measurement. The final result was thus:

$$\sigma_{Z\gamma^* \to qq\rho} = 0.090 \pm 0.033(stat) \pm 0.005(syst\ cut) \pm 0.014(bckg) pb,$$

in agreement with the Standard Model expectation of 0.082 pb. This result is very preliminary and has to be considered as a cross-check of the analysis presented in sec. 7.1.

8 Conclusions

In the data sample collected by the DELPHI detector at centre-of-mass energies ranging from 183 GeV to 208 GeV, the cross-sections for the production of $\mu^+\mu^- q\bar{q}$, $e^+e^- q\bar{q}$, $l^+l^-l^+l^-$, $\nu\bar{\nu}q\bar{q}$ and $q\bar{q}q\bar{q}$ (in the $q\bar{q}\rho$ case) final states have been measured and compared with the Standard Model expectations. In the $e^+e^- q\bar{q}$ channel the deviation from Standard Model observed in 1997-1999 statistics, was not confirmed by 2000 data. Preliminary measurements of the $Z\gamma^*$ contributions to the $l^+l^- q\bar{q}$, $l^+l^-l^+l^-$, $\nu\bar{\nu}q\bar{q}$ and $q\bar{q}q\bar{q}$ final states were performed and found to be in agreement with the Standard Model.

References

[1] A. Lipniacka *et al.*, DELPHI Collaboration, *Measurement of the production of four-fermion final states mediated by neutral current processes.*, contributed paper to XXXVI Rencontre de Moriond, Les Arcs (2001), DELPHI 2001-008 CONF 449.

[2] R. Contri *et al.*, DELPHI Collaboration, *Measurement of the production of four-fermion final states mediated by neutral current processes.*, contributed paper to the ICHEP2000 Conference, Osaka (2000), DELPHI 2000-141 CONF 440.

[3] R. Contri *et al.*, DELPHI Collaboration, *Measurement of the production of four-fermion final states mediated by non-ZZ neutral current processes.*, contributed paper to the HEP'99 Conference, Tampere (1999), DELPHI 99-68 CONF 255.

[4] R. Contri *et al.*, DELPHI Collaboration, *Measurement of the production of four-fermion final states mediated by neutral current processes.*, contributed paper to the XXXVth Rencontre de Moriond, Moriond (2000), DELPHI 2000-040 CONF 358.

[5] DELPHI Collaboration, *Measurement of ZZ production using data between* $\sqrt{s}$*=183 and 202 GeV*, contributed paper to ICHEP2000 OSAKA Conference, DELPHI 2000-145 CONF 444

[6] DELPHI Collaboration, P.Abreu *et al.*, Nucl. Instr. and Meth. **A378** (1996) 57.

[7] `DELSIM` *Reference Manual*, DELPHI note, DELPHI 87-97 PROG-100

[8] F.A. Berends, R. Pittau, R. Kleiss, Comp. Phys. Comm. **85** (1995) 437–452.

[9] T. Sjöstrand, Comp. Phys. Comm. **39** (1986) 347; T. Sjöstrand, `PYTHIA 5.6` *and* `JETSET 7.3`, CERN-TH/6488-92.

[10] Y.Kurihara, J. Fujimoto, T. Munehisa, Y. Shimizu, KEK CP-035, KEK 95-126 (1995).

[11] S.Nova, A.Olshevski, and T. Todorov, *A Monte Carlo event generator for two photon physics*, DELPHI note 90-35 PROG 152.

[12] F. A. Berends, P. H. Daverveldt, R. Kleiss, Comp. Phys. Comm. **40** (1986) 271-284, 285-307, 309-326

Peter Dornan, ALEPH Collaboration, private communication.

M.Felcini , A. Holzner, S.Shevchenko, M.Weber, L3 Collaboration, L3 Note 2485.

[13] S. Jadach,W. Placzek, M. Skrzypek, B.F. Ward and Z. Was. Comput. Phys. Commun. **119** (1999) 1.

[14] Maarten Boonekamp, KoralW for Delphi, DELPHI 2000-174 PROG 243.

[15] T. Sjöstrand, `PYTHIA 5.7` *and* `JETSET 7.4`, CERN-TH/7112/93 (1993).

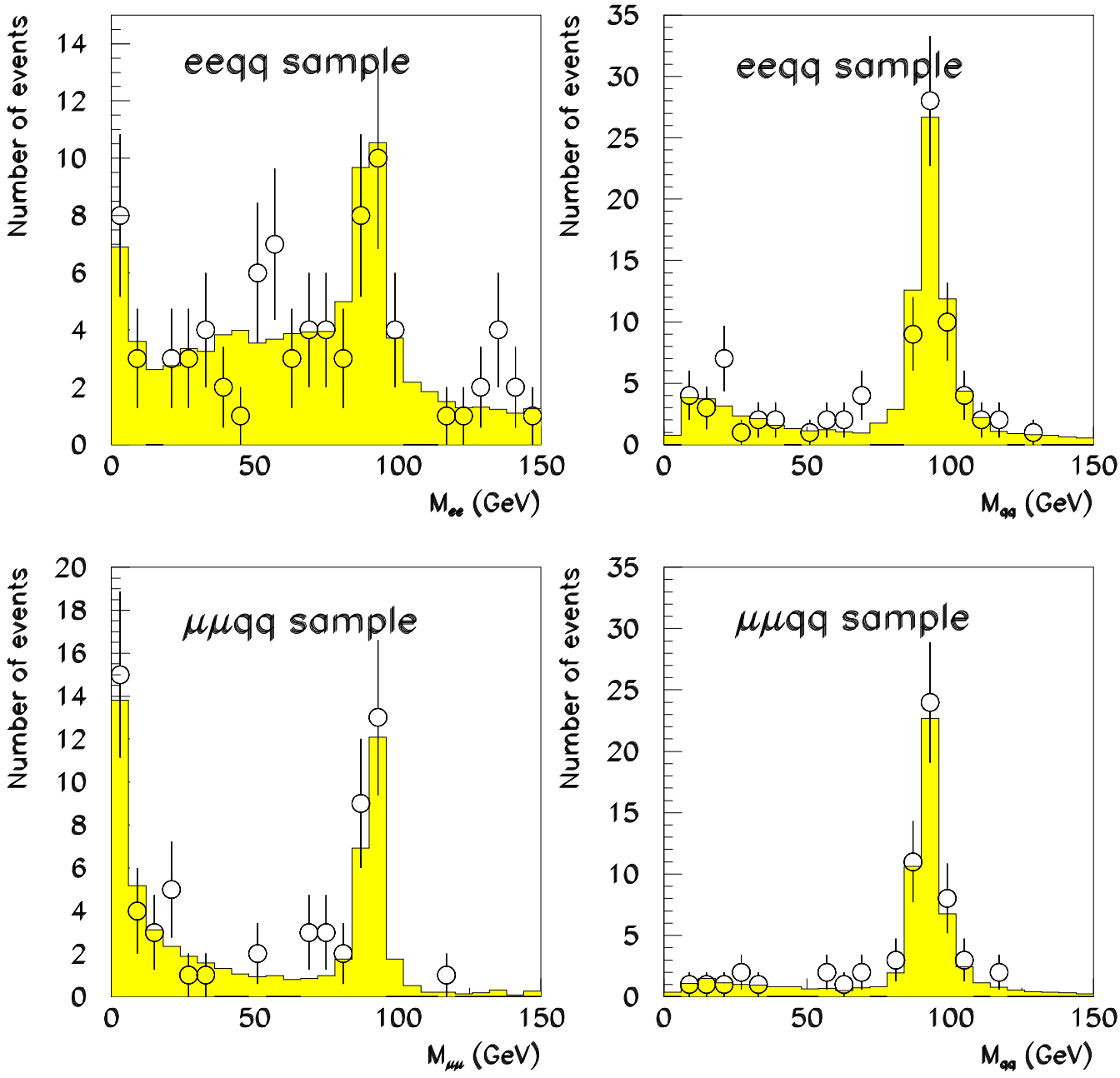

Figure 1: Fermion pair mass distributions in $l^+l^-q\bar{q}$ events. The points are the data, the histogram is the result of the fit.

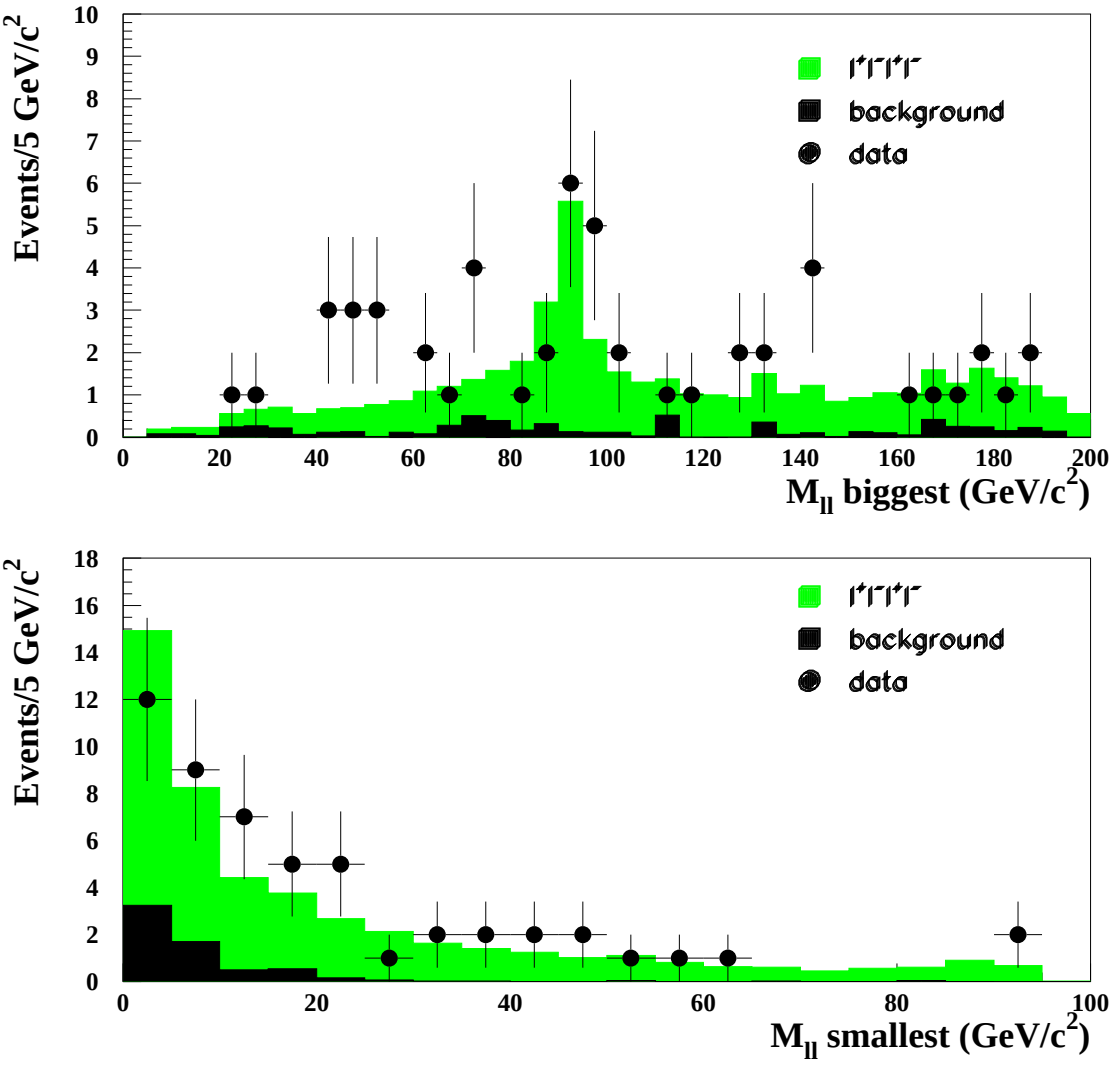

Figure 2: Mass distributions for pairs from charged four-lepton events. The dots are the data, the dark shaded histograms the Monte Carlo predictions for the background and the light shaded ones correspond to the Monte Carlo expected signal. Pairs are made of opposite charge leptons.

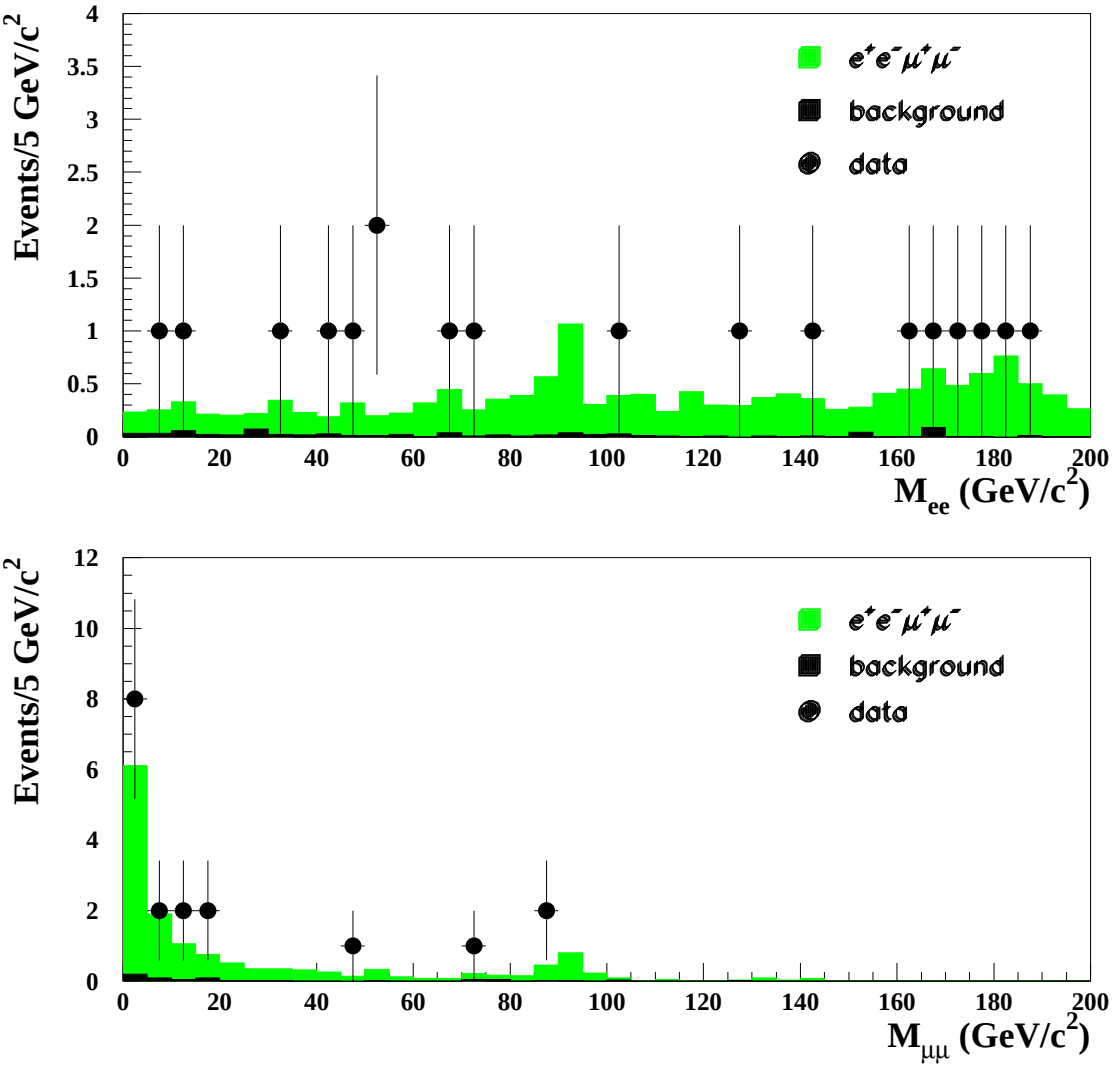

Figure 3: Mass distributions for pairs from $e^+e^-\mu^+\mu^-$ events. The dots are the data, the dark shaded histograms the Monte Carlo predictions for the background and the light shaded ones correspond to the Monte Carlo expected signal after particle identification.

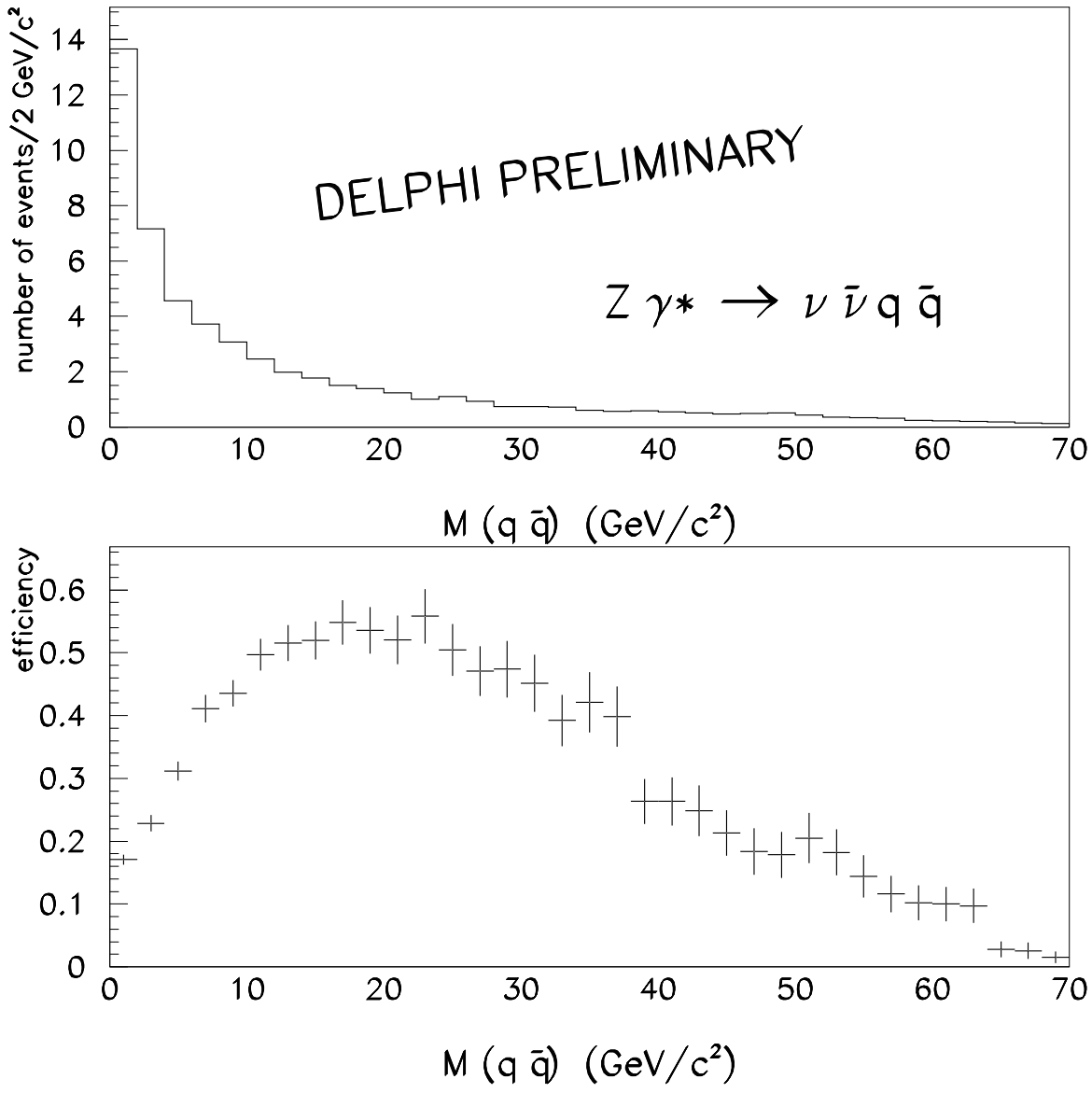

Figure 4: Expected mass distribution of $Z\gamma^* \to q\bar{q}\nu\bar{\nu}$ (upper plot). Selection efficiency of the analysis (lower plot)

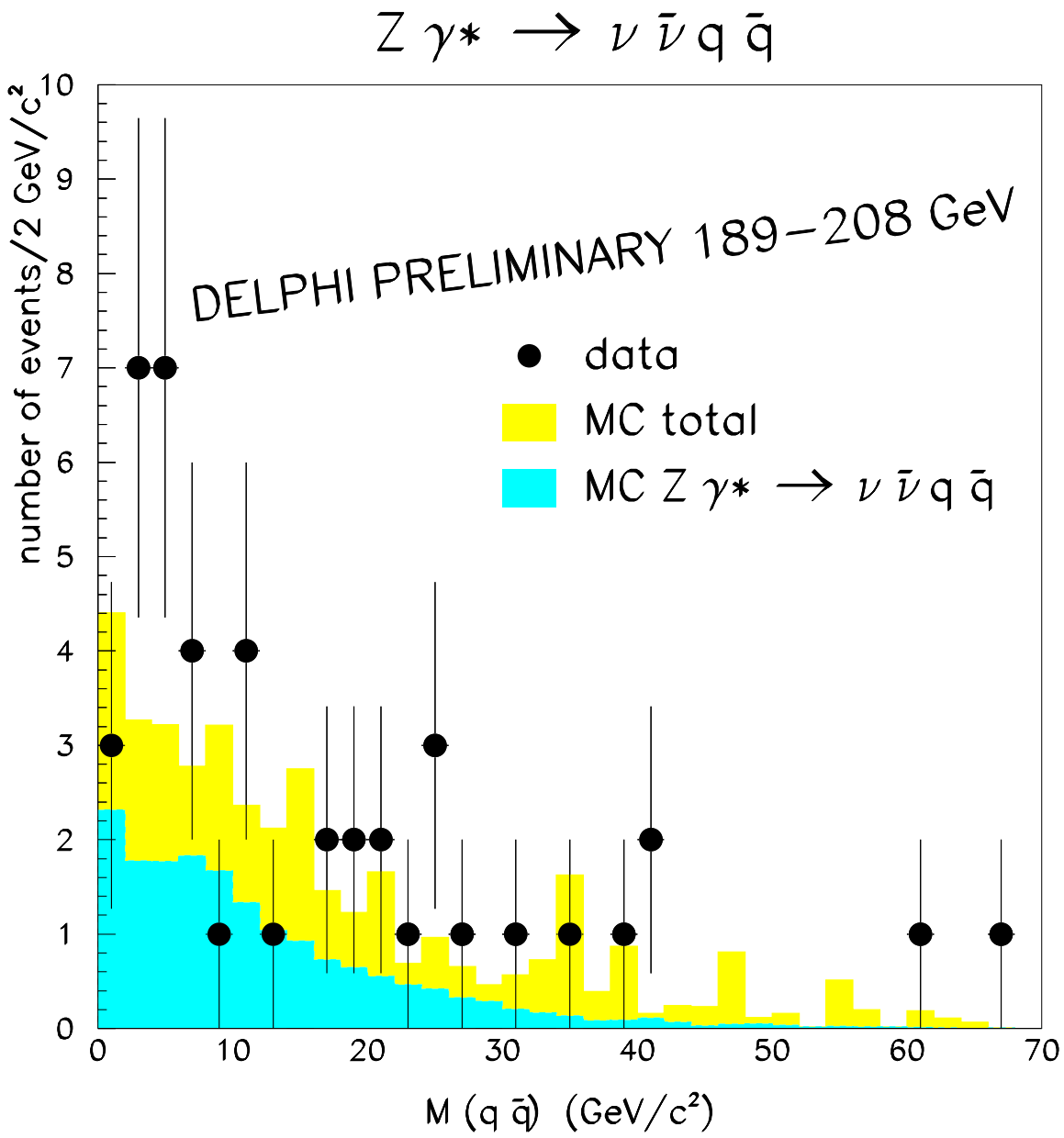

Figure 5: The distribution of the invariant mass of the hadronic system in the $\nu\bar{\nu}q\bar{q}$ selection. The black circles are the data, the dark histogram shows the signal contribution, and the light shaded histogram shows the total predicted spectrum.

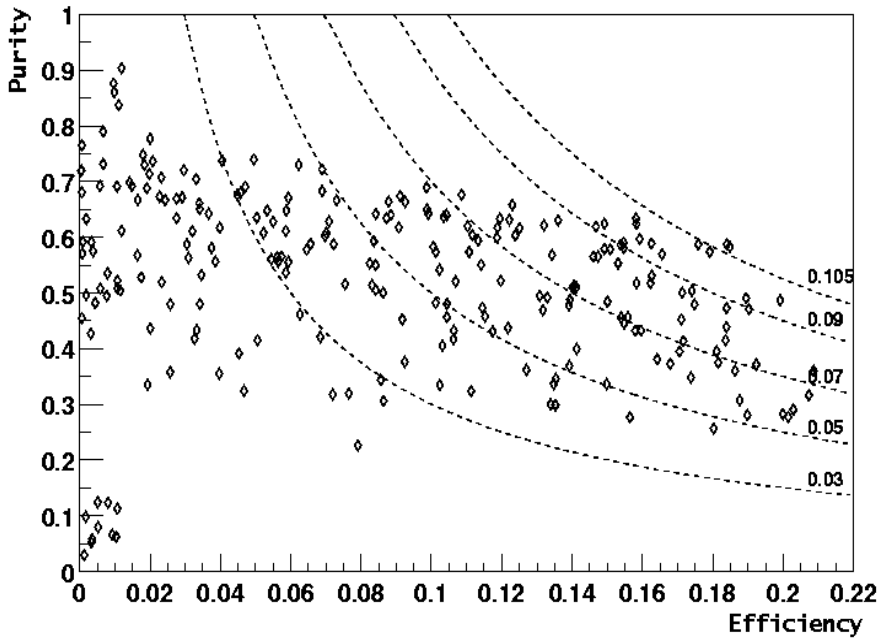

Figure 6: Efficiency-purity optimization process in the $q\bar{q}q\bar{q}$ channel (sec 7.1). The dotted lines represent different ϵp values.

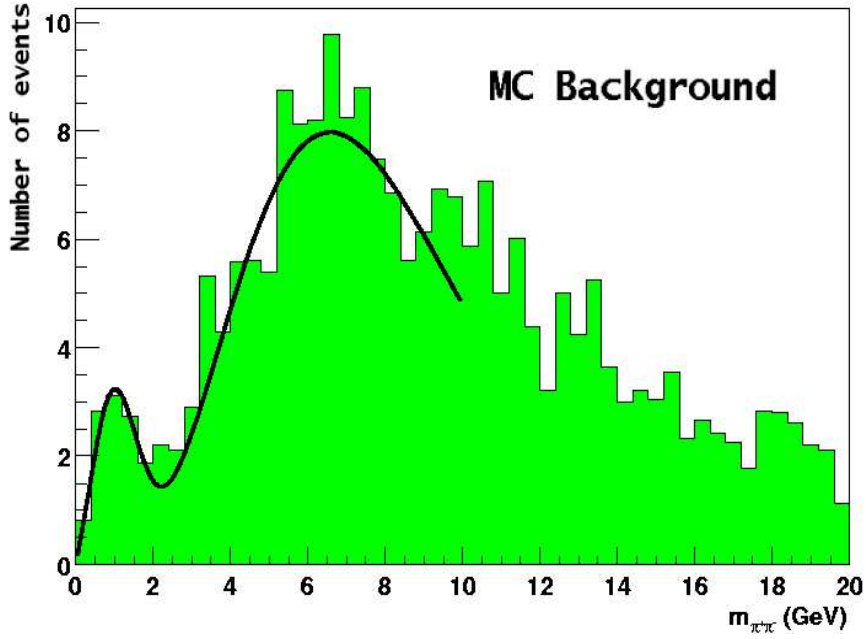

Figure 7: Simulated invariant mass distribution of $\pi^+\pi^-$ pair candidates considered as backgrounds to $e^+e^- \to Z\gamma^* \to qq\rho,\ \rho \to \pi^+\pi^-$.